

# Enhancing Scalability of Quantum Eigenvalue Transformation of Unitary Matrices for Ground State Preparation through Adaptive Finer Filtering

Erenay Karacan,<sup>1,\*</sup> Yanbin Chen,<sup>2,†</sup> and Christian B. Mendl<sup>2,3,‡</sup>

<sup>1</sup>*Technical University of Munich, CIT, Department of Electrical Engineering and Information Technology, Arcisstraße 21, 80333 Munich, Germany*

<sup>2</sup>*Technical University of Munich, CIT, Department of Computer Science, Boltzmannstraße 3, 85748 Garching, Germany*

<sup>3</sup>*Technical University of Munich, Institute for Advanced Study, Lichtenbergstraße 2a, 85748 Garching, Germany*

(Dated: June 25, 2024)

Hamiltonian simulation is a domain where quantum computers have the potential to outperform their classical counterparts due to their inherent quantum behavior. One of the main challenges of such quantum algorithms is up-scaling the system size, which is necessary to achieve meaningful quantum advantage. In this work, we present an approach to improve the scalability of eigenspace filtering for the ground state preparation of a given Hamiltonian. Our method aims to tackle limitations introduced by a small spectral gap and high degeneracy of low energy states. It is based on an adaptive sequence of eigenspace filtering through Quantum Eigenvalue Transformation of Unitary Matrices (QETU) followed by spectrum profiling. By combining our proposed algorithm with state-of-the-art phase estimation methods, we achieved good approximations for the ground state energy with local, two-qubit gate depolarizing probability up to  $10^{-4}$ . To demonstrate the key results in this work, we ran simulations with the transverse-field Ising Model on classical computers using `Qiskit`. We compare the performance of our approach with the static implementation of QETU and show that we can consistently achieve three to four orders of magnitude improvement in the absolute error rate.

## I. INTRODUCTION

A natural application field of quantum computers is calculating a given Hamiltonian's ground state and the corresponding energy. This task has extensive applications in quantum chemistry and condensed matter physics. Recently, an eigenspace filtering algorithm named "Quantum Eigenvalue Transformation of Unitary Matrices" (QETU) was proposed by Dong et al. [1] as enabled by the Quantum Signal Processing (QSP) framework [2]. There, the Hamiltonian block-encoding was substituted by the unitary time evolution operator, which is likely more straightforward to realize (via Trotterization) than the conventional block-encoding, particularly in the early fault-tolerant regime. This algorithm works well for systems where the following three assumptions are fulfilled: 1) The spectral gap  $\Delta$  between the ground and first excited state is large enough 2) A cut-off value  $\mu$  that bisects the ground state energy and first excited state energy can be guessed or estimated accurately 3) The overlap of the initial state with the ground state is large enough to achieve sensible success probabilities. Although starting with a high enough initial overlap remains a prerequisite for most existing algorithms, here we focus on the first two assumptions, which are difficult to fulfill as the system size scales up. The spectral gap  $\Delta$  is expected to decrease when studying higher-dimensional systems. In this situation, the QETU algorithm requires a correspondingly higher polynomial degree of the QSP

sequence to have a sharp enough transition. This, however, increases the gate count on the longest path significantly. In this work, we propose an adaptive set of finer filtering stages to alleviate the challenges introduced by the small spectral gap with a trade-off over increased total simulation time, where we keep the polynomial degree fixed.

In the simulations, we employed the Riemannian quantum circuit optimization (RQC-Opt) [3] algorithm for simulating the time evolution of the quantum system and ran the algorithms under different noise levels. Our results demonstrate that our approach can yield a final state whose overlap with the ground state is larger compared to the static repetition of QETU. When combined with efficient phase estimation methods, such as the Robust Phase Estimation algorithm proposed by Ni et al. [4] or the Quantum Complex Exponential Least Squares (QCELS) algorithm proposed by Ding et al. [5], we observe significant improvement in the approximation error compared to other similar ground state preparation methods with similar maximal simulation time.

The main idea of our work is to scale up the Hamiltonian to perform a "stretching" of the spectrum after each stage of applying QETU to achieve successively finer filtering. This idea necessitates estimating how much of the spectrum could be successfully filtered in the previous stages so that unwanted amplification of higher energy states can be avoided after the stretching. For this purpose, we employ the algorithm proposed by Lin and Tong [6]. This algorithm aims to approximate the Cumulative Distribution Function (CDF) of an input state (with respect to the given Hamiltonian) by employing the Fourier series approximation of the periodic error function in combination with its Fourier moments, which are

\* erenay.karacan@tum.de

† yanbin.chen@tum.de

‡ christian.mendl@tum.de

to be acquired through quantum simulations. We use this approach in our “profiling” stages to determine an updated spectrum length after each successful filtering.

## II. BACKGROUND

### A. Fundamentals of QETU

As stated in [1, Theorem 1] and visualized in Fig. 1, the QETU circuit with symmetric phases  $\vec{\phi} \in \mathbb{R}^{\eta+1}$  optimized for a target polynomial  $F(a)$  and applied to a given input state  $|\psi\rangle$  delivers the following final state, after the ancilla qubit is reset to  $|0\rangle$ :

$$\begin{aligned} \langle 0|_{\text{anc}} \mathcal{U}_{\text{QETU}} |0\rangle_{\text{anc}} |\psi\rangle &= \frac{F(\cos(\frac{H}{2})) |\psi\rangle}{\|\langle \psi | F(\cos(\frac{H}{2})) | \psi \rangle\|} \\ &= \frac{1}{\|\langle \psi | F(\cos(\frac{H}{2})) | \psi \rangle\|} \sum_j c_j F(\cos(\lambda_j/2)) |\psi_j\rangle, \end{aligned} \quad (1)$$

where  $\{\lambda_j, |\psi_j\rangle\}_j$  is the eigensystem of the Hamiltonian and  $c_j = \langle \psi | \psi_j \rangle$  is the overlap of the initial state with the eigenstate  $|\psi_j\rangle$ . Here,  $F(a)$  has to be real-valued, with parity  $\eta \bmod 2$ , maximum degree  $\eta$  and has to satisfy  $|F(a)| \leq 1$  for all  $a \in [-1, 1]$ .

### B. Eigenspace Filtering with QETU

With sensible estimates for the lower and upper bounds of the spectrum  $(\lambda_{\text{LB}}, \lambda_{\text{UB}})$ , we can ensure that the linearly transformed eigenspace is in the interval  $(0, \pi)$ . The linear transformation can be applied as:

$$\tilde{H} := \frac{\pi(H - \lambda_{\text{LB}})}{\lambda_{\text{UB}} - \lambda_{\text{LB}}}. \quad (2)$$

Then, the cosine transformation is strictly decreasing and maps the spectrum to  $(0, 1)$ . The overall transformation implies the following relation between the transformed  $a := \cos(\frac{\tilde{\lambda}}{2})$  space and  $\lambda$  space:

$$a_j := \cos\left(\frac{\pi(\lambda_j - \lambda_{\text{LB}})}{2(\lambda_{\text{UB}} - \lambda_{\text{LB}})}\right) \quad (3)$$

where  $\{\lambda_j\}_j$  is the spectrum of the Hamiltonian  $H$ . We now introduce the main task as follows:

**Objective 1** (Ground State Preparation). *Supposed we are given a Hamiltonian  $\tilde{H}$ , whose spectrum is contained in  $(0, \pi)$ , whose first excited state energy and ground state energy are separated by a spectral gap  $\Delta > 0$  and which can be accessed through its time evolution operator; the goal is to find an approximation  $|\psi_f\rangle$  of the ground state  $|\psi_0\rangle$ , such that  $|\langle \psi_0 | \psi_f \rangle| \geq 1 - \epsilon$ .*

Dong et al. [1] show that if we employ a QETU circuit where  $\tilde{H}$  is used in the time evolution operator and optimize the QSP phases for a polynomial  $F(a)$  with a step-like transition behavior from 0 to 1 at the cut-off value  $\mu \in (a_1, a_0)$ , we can amplify the overlap of any initial arbitrary state with the ground state and dampen the overlap with all excited states. An example of such a polynomial  $F(a)$  is given in Fig. 2.

However, a smaller spectral gap causes lower amplification. To get around this problem, the authors propose ([1, Theorem 6]) to scale the polynomial degree  $\eta$ , hence also the query depth of the time evolution operator as:

$$\tilde{\mathcal{O}}(\Delta^{-1} \log(\epsilon^{-1})) \text{ queries to the (controlled)-U} \quad (4)$$

This, however, implies that we have to arbitrarily increase the polynomial degree for an arbitrarily small spectral gap  $\Delta$  and/or error  $\epsilon$ . In turn, this increases the circuit depth significantly. An alternative, more efficient way is to apply QETU with (relatively) lower degree multiple times. This cuts down on the circuit depth, as the longest path is dominated by the ancilla qubit and this qubit is reset between each repetition of QETU. Hence, throughout the rest of the paper we retain a fixed polynomial degree. Moreover, we define a new set of parameters and metrics to assess the performance of this algorithm.

**Definition 1** (Relative Amplification). *The relative amplification between an initial state  $|\psi_{\text{init}}\rangle$  and a final state  $|\psi_f\rangle$ , in relation to the ground and first excited states, is defined as:*

$$A := \sqrt{\frac{\sum_j |\langle \psi_f | \psi_{0,j} \rangle|^2 / \sum_j |\langle \psi_{\text{init}} | \psi_{0,j} \rangle|^2}{\sum_j |\langle \psi_f | \psi_{1,j} \rangle|^2 / \sum_j |\langle \psi_{\text{init}} | \psi_{1,j} \rangle|^2}} \quad (5)$$

where  $\text{span}\{|\psi_{0,j}\rangle\}_j, \text{span}\{|\psi_{1,j}\rangle\}_j$  are the ground and first excited eigenspaces, respectively.

The relative amplification can be used as a strong indicator of state fidelity. If  $A \approx 1$ , the relation between the ground and first excited state overlaps remains approximately the same after the amplification. For  $A \rightarrow \infty$  we can infer that  $|\langle \psi_f | \psi_1 \rangle| \rightarrow 0$ . This also indicates that for all other excited states  $|\langle \psi_f | \psi_j \rangle| \rightarrow 0, \forall j > 1$ . This results from the monotonously increasing nature of  $F(a)$ , for the  $a$  values mapped into the step-like transition interval and we assume that outside of the transition interval  $F(a)$  oscillates with a negligible amplitude. Hence,

$$A \rightarrow \infty \implies |\langle \psi_f | \psi_0 \rangle| \rightarrow 1. \quad (6)$$

With this performance metric, we re-formulate the main objective as:

**Objective 2** (Ground State Overlap Amplification). *With the same assumptions from Obj. 1 and Def. 1, the goal is to prepare a quantum state  $|\psi_f\rangle$  with a relative amplification  $\tilde{A}$ , that scales as:*

$$n_1 \frac{a_0}{\Delta_a \tilde{\epsilon}} \leq \tilde{A} \leq n_2 \frac{a_0}{\Delta_a \tilde{\epsilon}} \quad (7)$$

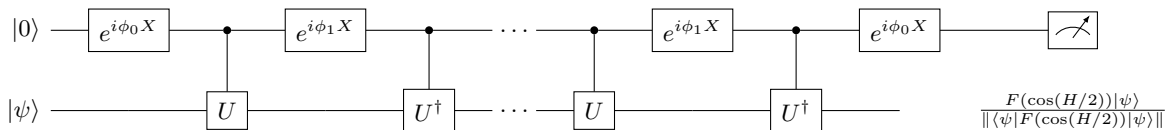


FIG. 1. Quantum Eigenvalue Transformation of Unitary Matrices (QETU) Circuit in compact notation where  $U$  is the multi-qubit gate applying the time evolution operator  $U = e^{-iH}$ , acting on all the system qubits and the X-Rotation gates are applied to the ancilla qubit. Symmetric phases  $(\phi_0, \phi_1, \dots, \phi_1, \phi_0) \in \mathbb{R}^{\eta+1}$  are optimized for a given target polynomial  $F(a)$ .

where  $\tilde{\epsilon} \ll 1$  is the "inverse amplification strength",  $n_1, n_2 > 0$  and  $\Delta_a := a_0 - a_1$  is the spectral gap in the cosine space.

Inverse Amplification Strength  $\tilde{\epsilon}$  can be taken as an indicator for the final state infidelity  $\epsilon$  as given in Obj. (1). Throughout rest of this article, we will use this parameter to represent the error of our main objective.

Obj (2) can be achieved by repeating the QETU circuit consecutively  $\gamma$  times, which increases the maximal simulation time  $T_{\max}$  by  $\gamma$ .

**Definition 2** (Maximal Simulation Time). *Maximal simulation time of a Hamiltonian simulation circuit is defined as:*

$$T_{\max} = \sum_j t_j \quad (8)$$

where  $\{t_j\}_j$  are the time steps of each time evolution operator  $U_j = e^{-iHt_j}$  employed in the quantum circuit.

Moreover, we formalize the circuit depth through the following definition:

**Definition 3** (Circuit Depth). *Circuit depth required for a ground state overlap amplification process (using QETU with polynomial  $F(a)$  and spectrum bounds  $\lambda_{LB}, \lambda_{UB}$ ) is given as the constant factor  $\gamma$ , which scales the maximal simulation time  $T_{\max}$  as:*

$$T_{\max} = \gamma \eta \frac{\pi}{\lambda_{UB} - \lambda_{LB}} \quad (9)$$

where  $\eta$  is the degree of the polynomial  $F(a)$ .

**Proposition.** *A final state  $|\psi_f\rangle$  with relative amplification  $\tilde{A}$  (satisfying Eq. (7)) can be achieved by applying QETU on an initial state  $|\psi_{\text{init}}\rangle$  repeatedly  $\lceil \gamma_{ST} \rceil$  times, where circuit depth  $\gamma_{ST}$  (as defined in Def. 3) scales as:*

$$\gamma_{ST} = \Theta(\Delta^{-1} \log(\Delta^{-1} \tilde{\epsilon}^{-1})) \quad (10)$$

where  $\Delta = \lambda_1 - \lambda_0$  is the spectral gap and  $\tilde{\epsilon}$  is the inverse amplification strength.

For the proof of the proposition, please refer to Appendix A.

It is also worth stating that the initial overlap problem persists with this method, manifesting itself as causing a low success probability for the amplification, if the overlap of the initial state with the ground state is low. In our

simulations, we randomize the initial state and limit the number of measurements performed on the ancilla qubit proportional to the success probability of each ancilla qubit being reset to  $|0\rangle$ . A much more effective method could be using another quantum oracle to achieve an initial state whose overlap with the ground state is increased compared to randomized initialization.

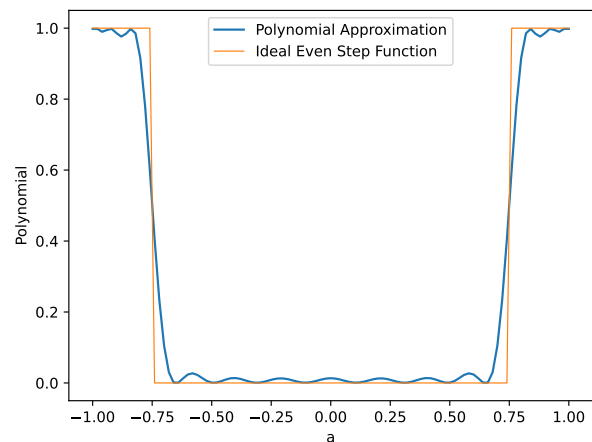


FIG. 2. Example polynomial  $F(a)$  of degree 30, as an approximation of the even step function with cut-off value  $\mu = 0.75$ . Chebyshev polynomials of the second kind were used as basis. Convex optimization library "cvxpy" was used to optimize coefficients of the Chebyshev polynomials

### C. Spectrum Profiling

In this section we summarize how the Cumulative Distribution Function (CDF) of the Hamiltonian is approximated, which will later be used in the profiling stage of the Adaptive Finer Filtering. As proposed by Lin & Tong [6], given the Hamiltonian  $H$  with the spectrum  $\{\lambda_j, |\psi_j\rangle\}_j$ , the CDF of the input state  $|\psi_{\text{init}}\rangle$  is defined in the following way:

$$C(x) := \sum_{j: \lambda_j \leq x} |\langle \psi_{\text{init}} | \psi_j \rangle| \quad (11)$$

If we have access to lower and upper bounds for the spectrum  $(\lambda_{UB}, \lambda_{LB})$ , hence also to an upper bound for the

spectrum length  $\Lambda := \lambda_{\text{UB}} - \lambda_{\text{LB}}$ , we can approximate (a periodic repetition of) CDF as the convolution of the  $\Lambda$ -periodic continuation of the error function  $\text{erf}_\Lambda(x)$  and the spectral density  $p(x) := \sum_j |\langle \psi_{\text{init}} | \psi_j \rangle| \delta(x - \lambda_j)$ :

$$C(x) \approx (\text{erf}_\Lambda * p)(x), \quad \forall x \in (\lambda_{\text{LB}}, \lambda_{\text{UB}}). \quad (12)$$

Furthermore, we can approximate  $\text{erf}_\Lambda$  by a Fourier series expansion with  $(2D+1)$ -terms:

$$\text{erf}_\Lambda(x) \approx \sum_{|k| \leq D} F_k e^{ikx}, \quad (13)$$

where  $F_k$  are the Fourier coefficients. From this, it follows that:

$$C(x) \approx \sum_{|k| \leq D} F_k e^{ikx} \langle \psi_{\text{init}} | e^{-ikH} | \psi_{\text{init}} \rangle \quad (14)$$

where the Fourier moments  $\langle \psi | e^{-ikH} | \psi \rangle$  can be efficiently acquired through quantum simulation by employing a simple Hadamard test circuit, as shown in Fig. 4. For the case  $\Lambda = 2$ , the Fourier coefficients read [7]:

$$F_0 = \frac{1}{2} \quad (15a)$$

$$F_{2j+1} = -i \sqrt{\frac{\beta}{2\pi}} e^{-\beta} \frac{I_j(\beta) + I_{j+1}(\beta)}{2j+1} \quad (15b)$$

$$F_D = -i \sqrt{\frac{\beta}{2\pi}} e^{-\beta} \frac{I_{\lfloor \frac{D-1}{2} \rfloor}(\beta)}{D} \quad (15c)$$

where  $j \in \{\lfloor \frac{-D-1}{2} \rfloor, \dots, 0, \dots, \lfloor \frac{D-3}{2} \rfloor\}$ ,  $I_n$  is the  $n$ -th modified Bessel function of the first kind and  $\beta$  to be chosen depending on the target approximation precision, with a trade-off of larger contribution from the higher order Fourier terms. It is important to note that  $F_{2k} = 0$ , hence we need to compute only  $\lfloor \frac{D-1}{2} \rfloor$  Fourier moments through quantum simulation, which alleviates the total simulation time on the quantum hardware.

### III. ADAPTIVE FINER FILTERING

As we scale up the system size, eigenspace filtering with QETU can face practical difficulties due to a decreasing spectral gap, as a small  $\Delta$  increases the circuit depth  $\gamma$  (as defined in Def. 3) and also makes choosing a cut-off value  $\mu$  difficult. In this section, we propose an algorithm to circumvent these challenges. Our goal is to achieve the following

**Objective 3** (Adaptive Finer Filtering (AFF)). *With the assumptions from Def. 2, we aim to achieve relative amplification  $\tilde{A}$  satisfying the condition in Eq. 7, while the circuit depth  $\gamma_{\text{AFF}}$  scales as:*

$$\gamma_{\text{AFF}} = \Theta(\Delta^{-1}) \quad (16)$$

*in relation to the spectral gap  $\Delta$ , independent of amplification strength  $\tilde{\epsilon}^{-1}$ .*

The approach introduced in this paper achieves this goal by employing a profiling stage with the aforementioned algorithm by Lin and Tong [6] to estimate new upper and lower bounds for the spectrum after the filtering and by performing further filtering on a ‘‘stretched’’ Hamiltonian, depending on the new bounds.

In the profiling stage, updated spectrum bounds are taken as boundaries of the interval where the growth rate of the CDF is the highest. This is determined by the region where the first derivative of the CDF is greater than  $\xi_1$  and the absolute value of the second derivative is smaller than  $\xi_2$ . Here  $(\xi_1, \xi_2)$  are user-set parameters that can be determined depending on the acquired CDF.

A systematic summary of the Adaptive Finer Filtering Algorithm and its helper method for the profiling stage can be found in Algorithms 1 and 2. To see how we achieve the target scaling in Eq. (16), refer to Appendix B. We also note that the scaling given in Eq. (16) achieves the optimal  $\Delta$ -scaling, as shown in [8].

---

#### Algorithm 1: Adaptive Finer Filtering for Ground State Preparation

---

**Data:**  $|\psi_{\text{init}}\rangle, \lambda_{\text{UB}}^0, \lambda_{\text{LB}}^0, \mu^0, \eta, \vec{m}, M, \xi_1, \xi_2, D$   
**Ensure:**  $\lambda_j \in [\lambda_{\text{LB}}^0, \lambda_{\text{UB}}^0], \forall j \in \{0, \dots, 2^L - 1\}; \eta$  is even;  $\vec{m} = (m_0, \dots, m_{M-1})$   
 $|\psi^0\rangle \leftarrow |\psi_{\text{init}}\rangle$   
**for**  $i = 0 \dots M - 1$  **do**  
     $|\psi^{(i+1)}\rangle \leftarrow \text{QETU}(|\psi^i\rangle, \mu^i, \eta, \lambda_{\text{LB}}^i, \lambda_{\text{UB}}^i)$   
    // With linear transformation as in Eq. 2  
     $\lambda_{\text{LB}}^{(i+1)}, \lambda_{\text{UB}}^{(i+1)} \leftarrow \text{SP}(|\psi^{(i+1)}\rangle, \lambda_{\text{LB}}^i, \lambda_{\text{UB}}^i, \xi_1, \xi_2, D)$   
    // Algorithm 2  
     $\Lambda^{(i+1)} \leftarrow \lambda_{\text{UB}}^{(i+1)} - \lambda_{\text{LB}}^{(i+1)}$   
     $c_1^{(i+1)} \leftarrow \frac{\pi}{2\Lambda^{(i+1)}}$   
     $c_2^{(i+1)} \leftarrow -c_1^{(i+1)} \lambda_{\text{LB}}^{(i+1)}$   
     $\mu^{(i+1)} \leftarrow \cos(c_1^{(i+1)}(\lambda_{\text{LB}}^{(i+1)} + \frac{\Lambda^{(i+1)}}{m_i}) + c_2^{(i+1)})$   
**end**  
**return**  $|\psi^M\rangle$

---



---

#### Algorithm 2: Spectrum Profiling (SP)

---

**Data:**  $|\psi\rangle, \lambda_{\text{UB}}, \lambda_{\text{LB}}, \xi_1, \xi_2, D$   
**Ensure:**  $\langle \psi_j | \psi \rangle \approx 0, \forall \lambda_j \notin [\lambda_{\text{LB}}, \lambda_{\text{UB}}]; \xi_1, \xi_2 > 0$   
 $\Lambda \leftarrow \lambda_{\text{UB}} - \lambda_{\text{LB}}$   
 $\tilde{H} \leftarrow \frac{2}{\Lambda}(H - \lambda_{\text{LB}}I) - I$  // Ensures  $\tilde{\lambda} \in (-1, 1)$   
 $x \leftarrow (-1, \dots, 1)$  // energy grid  
 $C(x) \leftarrow \sum_{k=-D}^D F_k e^{ikx} \langle \psi | e^{-ik\tilde{H}} | \psi \rangle$   
    // Through Hadamard tests and Eqs. (15)  
 $C'(x) \leftarrow \frac{d}{dx} C(x)$   
 $C''(x) \leftarrow \frac{d^2}{dx^2} C(x)$   
 $(x_{\text{LB}}, x_{\text{UB}}) \leftarrow (x_1, x_2),$   
    s. t.  $C'(x) > \xi_1 \wedge |C''(x)| < \xi_2, \forall x \in [x_1, x_2]$   
**return**  $\frac{\Lambda}{2}(x_{\text{LB}} + \frac{2\lambda_{\text{LB}}}{\Lambda} + 1), \frac{\Lambda}{2}(x_{\text{UB}} + \frac{2\lambda_{\text{LB}}}{\Lambda} + 1)$

---

In Alg. 1,  $\mu^0$  is the first cut-off value of the filtering sequence and can be set to a value between  $(0.9, 0.95)$ , in

practice. If the error margins for the estimates  $\lambda_{\text{LB}}^0$ ,  $\lambda_{\text{UB}}^0$  (initial lower and upper bounds for the whole spectrum) are too large, one can perform spectrum profiling with arbitrarily high/low bounds on the initial state before the first filtering stage to determine the bounds and  $\mu^0$  more accurately.

The number of initial filtering stages  $M - 1$ , polynomial degree for QETU  $\eta$ , division coefficient at each finer filtering stage  $\bar{m}$ , precision bounds for the spectrum profiling  $\xi_1, \xi_2$  and number of Fourier terms  $D$  are to be chosen depending on the system size, degeneracy of the Hamiltonian and initial overlap  $\langle \psi_{\text{init}} | \psi_0 \rangle$ .

An important distinction in this amplification process is that Eq. (6) does not directly hold anymore for a stretched Hamiltonian, as the spectrum cannot be mapped to the cosine space bijectively. That is why we require initial filtering stages (the number of which is given as  $M - 1$  in Alg. 1). These initial filtering stages stretch the Hamiltonian by a factor  $\gamma_j = \Theta(\Delta_j^{-1})$ , where

$$\Delta_j := a_0 - a_j, \quad j > 1 \quad (17)$$

is the  $j^{\text{th}}$ -higher spectral gap.

Consequently, initial filtering stages bring additive factors to the circuit depth as:  $\gamma_{\text{AFF}} = \Theta(\Delta^{-1} + \sum_{\Delta_j \in B} \Delta_j^{-1})$ , where  $B$  is the subset of higher spectral gaps with number of elements  $M - 1$ , each element of which corresponds to an initial filtering stage.

If we assume that the spectrum is evenly spread out in the cosine space, and the  $\eta, \mu$  parameters of each initial filtering stage are chosen such that we acquire  $1/\ell$  of the spectrum after each filtering, we would need

$$M = \lceil \log_{\ell} N \rceil \quad (18)$$

initial filtering steps, where  $N$  is the number of dimensions of the Hamiltonian. With the same assumptions as above, we can define the higher spectral gaps that make up the subset:

$$B = \{\Delta_{\lceil N/\ell^j \rceil}\}_{j=0}^{M-2}. \quad (19)$$

For our circuit depth (as given in Eq. (16) and derived in Appendix B), we ignore these additive factors with the assumption of  $\Delta \ll \Delta_j \quad \forall \Delta_j \in B$ , which is the case for most of the Hamiltonians of interest.

Another general problem of the algorithm given in Section II B is to find the cut-off value  $\mu$  accurately. In our approach, the profiling stage helps us to choose  $\mu$ , such that  $\tilde{\mu} := 2 \arccos(\mu)$  cuts the spectrum into two as:

$$\tilde{\mu} = c_1 \left( \lambda_{\text{LB}} + \frac{\Lambda}{m} \right) + c_2, \quad (20)$$

where  $\lambda_{\text{LB}}$  is the lower bound of the (filtered) spectrum,  $\Lambda$  is the total length of the (filtered) spectrum and the  $(c_1, c_2)$  coefficients are chosen according to the linear transformation shown in Eq. (2).

In order to reduce the possibility of  $\mu$  being greater than  $a_0$ , one can choose  $m$  adaptively. This case is unlikely in the early stages, so one can choose a larger  $m$

to cut off the spectrum into a smaller piece in order to increase effectiveness. In later stages,  $m$  can be chosen as 2 to avoid overfiltering ( $\mu > a_0$ ).

#### IV. SIMULATION RESULTS

To investigate the performance of our approach, we ran a set of simulations using IBM `qiskit`. The source code of our implementation is available at Ref. [9].

We primarily investigated the (integrable) transverse-field Ising Model (TFIM) governed by the Hamiltonian

$$H_{\text{TFIM}} = -J \sum_{j=1}^{L-1} Z_j Z_{j+1} - g \sum_{j=1}^L X_j. \quad (21)$$

Moreover, we implemented the QETU circuit with the control-free implementation of the time evolution circuit, as demonstrated in [1, Section VI].

For encoding the time evolution operator, we employed classical optimization through RQC-Opt [3]. This toolbox uses the Riemannian trust region algorithm to optimize the two-qubit gates in a brick wall circuit layout to approximate the time evolution operator of a given Hamiltonian. A central idea of this approach is to optimize the gates for smaller systems and use these same gates to represent the time evolution operator of a larger system, assuming translation invariant Hamiltonians. Particularly for the TFIM model, it reaches good approximations with relatively short circuit depths. In this work, we set the Hamiltonian coefficients as  $J = 1$  and  $g = 1$ .

Heuristically, we fix the  $(D, \beta, \xi_1, \xi_2)$  parameters to  $(7, 5, 0.03, 0.02)$  for system sizes  $L = 6, 8, 10$ . It is important to adjust these parameters for different system sizes and Hamiltonian parameters, depending on the required sharpness of the error function (determined by  $D$  and  $\beta$ ) and the values of  $C'(x), C''(x)$  (for  $\xi_1$  and  $\xi_2$ ). Remarkably, we can get a spectrum profile for this choice of low  $D$  by running the Hadamard sampling given in Fig. 4 only four times (for each time we execute Alg. 2). Namely, for even  $k$ ,  $F_k = 0$ , and for negative  $k$ , we can conjugate the Fourier moment estimated for  $-k$ .

Example plots for  $C(x)$  and its derivatives  $C'(x), C''(x)$  are visualized in Fig. 3. There one can spot the interval where the growth rate of the CDF is large. This interval is determined by the local maximum of the first derivative. We also demonstrate the amplification process in Table I for the system sizes  $L \in \{6, 8\}$  and  $J = 1, g = 1$ .

To test the success of our algorithm in estimating the ground state energy, we combine Adaptive Finer Filtering with Robust Phase Estimation (RPE), developed by Ni et al. [4], Direct Expectation Value Measurement as proposed by Dong et al. [1] and Quantum Complex Exponential Least Squares (QCELS) algorithm as developed by Ding et al. [5]. Results of the simulations with RPE and QCELS are demonstrated in Figure 5. For further

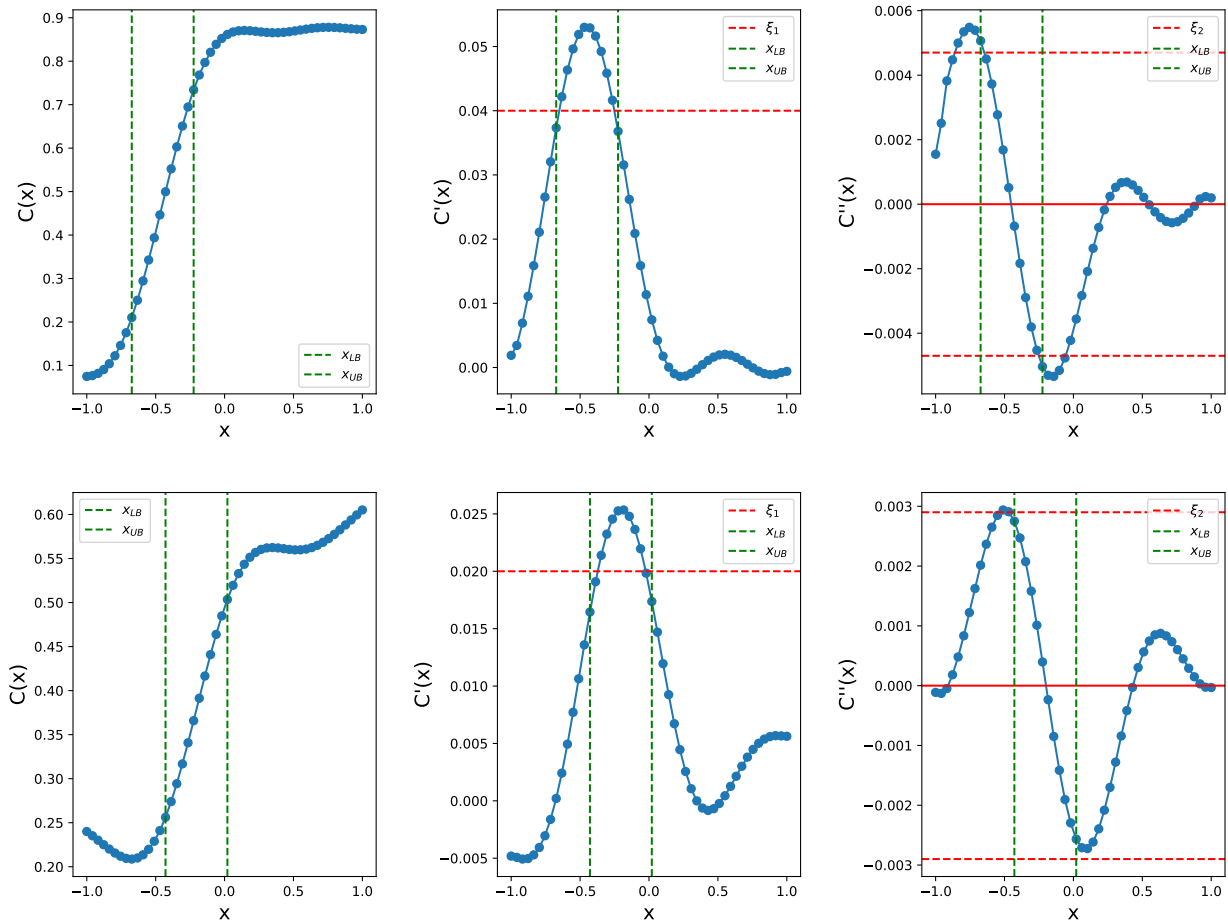


FIG. 3. Example plots of cumulative distribution functions (CDF) from the first (top) and second (bottom) filtering stages, plotted next to its first and second derivatives. Fourier moments were acquired through Hadamard sampling (Fig. 4), using  $10^3$  shots and simulated with a local depolarizing probability of  $10^{-3}$  for the two-qubit gates. Red horizontal lines represent precision bounds for the spectrum profiling  $\xi_1, \xi_2$ , and green vertical lines represent new upper/lower spectrum bounds resulting from the spectrum profiling. The Hamiltonian is the TFIM with system size  $L = 6$  and parameters  $J = 1, g = 1$ . For the top graph:  $(D, \beta, \lambda_{LB}, \lambda_{UB}) = (7, 5, -10, 10)$  and the input state  $|\psi\rangle$  was taken as the result of the initial filtering by QETU with  $\eta = 14, \mu = 0.95$ , applied to a randomized state  $|\psi_{init}\rangle$ . For the bottom graph:  $(D, \beta, \lambda_{LB}, \lambda_{UB}) = (7, 5, -8.78, -1.43)$  and the input state  $|\psi\rangle$  was taken as the result of the secondary filtering by QETU with  $\eta = 14, \mu = 0.92$ , applied to the result of the initial filtering.

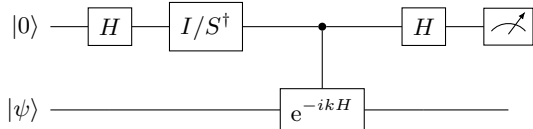


FIG. 4. Hadamard test circuit used to compute the Fourier moments in Eq. (14). The identity  $I$  is inserted to compute  $\text{Re} \langle \psi | e^{-ikH} | \psi \rangle$  and the conjugated phase gate  $S^\dagger$  is used to compute  $\text{Im} \langle \psi | e^{-ikH} | \psi \rangle$ .

details on the implementation of these algorithms, you can refer to Appendix C, D, and E. The best results acquired through simulations are displayed in Table II.

For the system size  $L = 10$ , we investigated a par-

ticularly challenging scenario, where  $\sum_j |\langle \psi_j | \psi \rangle| \approx 10^{-7}$  for  $|\psi_j\rangle$  being the first  $2^4$  low energy eigenstates. This increases the number of initial filtering stages  $M - 1$ , which might cause unwanted amplification of higher energy states. This can be solved by applying the same QETU circuit from the first filtering stage once more at the end. An example demonstration of this phenomenon is given in Fig. 6.

## V. DISCUSSION

By combining spectrum profiling through approximating the CDF and eigenspace filtering through QETU, we demonstrate how to alleviate large circuit depth scaling caused by a small spectral gap and get around the uncer-

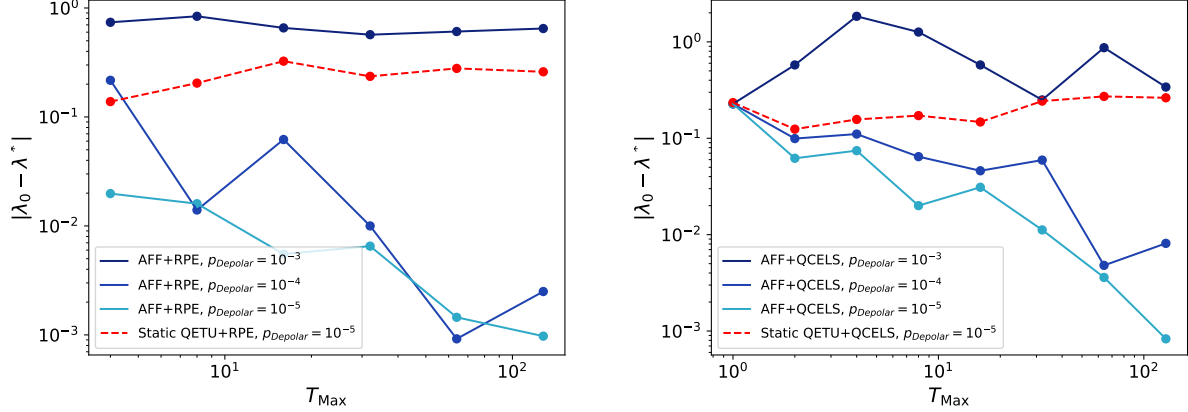


FIG. 5. Ground state energy estimation using Adaptive Finer Filtering (AFF), combined with Robust Phase Estimation [4] (left) and QCELS [5] (right). For comparison, the performance of statically applying QETU with the same number of repetitions  $M = 3$  and combining it with RPE / QCELS is plotted alongside in each graph. Simulations were conducted with  $10^4$  (of which around 1% corresponds to successful amplification) shots on the ancilla qubit per real and imaginary part of the targeted phase. The TFIM model with system size  $L = 6$  and system parameters  $J = 1, g = 1$  (Spectral gap  $\Delta \approx 0.263$ ) was used. Here,  $p_{\text{Depolar}}$  represents the local depolarizing probability of two-qubit gates. The depolarizing probability of single-qubit gates is taken as  $p_{\text{Depolar}}/10$ .

#### Ground State Preparation through Adaptive Finer Filtering

$$L = 6; \quad \lambda_0 \approx -7.7274$$

$i$	$\lambda_{\text{LB}}$	$\lambda_{\text{UB}}$	$\mu$	$p$	$ \langle \psi_0   \psi_f \rangle $
0	-10	10	0.95	0.053	0.243
1	-8.78	-1.43	0.92	0.362	0.568
2	-8.17	-6.98	0.7	0.502	0.996

$$L = 8; \quad \lambda_0 \approx -10.251$$

$i$	$\lambda_{\text{LB}}$	$\lambda_{\text{UB}}$	$\mu$	$p$	$ \langle \psi_0   \psi_f \rangle $
0	-15	15	0.95	0.007	0.289
1	-12.55	-5.2	0.7	0.6146	0.664
2	-10.75	-9.25	0.8	0.58	0.978

TABLE I. Amplification stages, demonstrated for TFIM with  $J = 1, g = 1$ , system sizes  $L = 6$  and  $L = 8$  (spectral gap in the cosine space:  $\Delta_a := a_0 - a_1 \approx 0.004$  and  $\Delta_a \approx 0.003$ ). Between stages, Spectrum Profiling (Alg. 2) was used in order to determine  $(\lambda_{\text{LB}}, \lambda_{\text{UB}})$  of the next stage. The initial cut-off value  $\mu^0$  was set to 0.95.  $p$  in the Table represents the success probability of resetting the ancilla qubit to  $|0\rangle$ . The initial state was randomized with an overlap of  $|\langle \psi_0 | \psi_{\text{init}} \rangle| \approx 0.014$  and 0.002 for  $L = 6$  and  $L = 8$  respectively. Compared to our method, repeating the first QETU layer ( $i = 0$ ) statically by the same number of times  $M = 3$  results in an overlap of  $\approx 0.62$  and  $\approx 0.35$ , respectively.

tainty of choosing an accurate cut-off value  $\mu$ , assuming that the time evolution operator can be realized by a relatively shallow circuit. Notably, our approach eliminates the dependence on the amplification strength  $\tilde{\epsilon}^{-1}$ . These

#### Ground State Energy Estimation through Adaptive Finer Filtering

$p_{\text{Depolar}}$	DEM	QCELS	RPE
$10^{-3}$	0.668	0.25	0.608
$10^{-4}$	0.472	0.0048	$9.2 \cdot 10^{-4}$
$10^{-5}$	0.579	$8.3 \cdot 10^{-4}$	$9.7 \cdot 10^{-4}$

TABLE II. Absolute error in approximating the ground state energy of the TFIM Hamiltonian ( $L = 6, J = 1, g = 1, \lambda_0 \approx -7.727$ ) using Direct Expectation Value Measurement (DEM), QCELS [5] and RPE [4]. We present results from ground state preparation through Adaptive Finer Filtering (AFF) (parameters kept same as in Table I).  $p_{\text{Depolar}}$  represents the local, two-qubit depolarizing probability, whereas single-qubit depolarizing probability was taken as  $\frac{p_{\text{Depolar}}}{10}$ . DEM was conducted with  $10^4$  samplings on all qubits. RPE and QCELS were conducted with  $10^4$  samplings on the ancilla qubit per each targeted phase. Simulations ran up to maximal simulation time  $T_{\text{Max}} = 2^7$ .

are important steps for the up-scaling of eigenspace filtering algorithms. Scalability is a general challenge for quantum technology, but conversely, it is one of the essential traits required by quantum algorithms to enable quantum advantage over classical counterparts.

The need for a large enough initial overlap  $\langle \psi_0 | \psi_{\text{init}} \rangle$  still persists, so that the success probability of amplification is sensibly high. For example, the end result demonstrated in Table I suggests a cumulative probability of around 0.75% that the end state after the third amplification stage can be achieved. This low probability comes from the fact that the initial state was randomized and, hence, did not have a high overlap with low-energy states.

Bearing this limitation in mind, we ran our simulations with a realistic, limited amount of shots ( $10^4$  to  $10^5$ ). We observe that most ( $\approx 99\%$ ) of the total capacity to perform measurements on the ancilla qubit, results in the ancilla qubit being reset to  $|1\rangle$  during one of the amplification stages. Despite this, we can still achieve the results demonstrated in Fig. 5 by employing RPE or QCELS.

Another important point is the total simulation time of the ground state preparation process. Although our approach decreases the maximal simulation time for  $\tilde{\epsilon} \ll 1$ , it causes an increase in the total simulation time as we introduce intermediate Hadamard sampling between amplification layers to perform the spectrum profiling. In practice, doing four samplings by setting the number of Fourier terms to  $D = 7$  delivers good results.

## VI. CONCLUSION AND OUTLOOK

As quantum computers are becoming able to accommodate more qubits and have the potential to outperform classical computers for certain tasks, quantum algorithms should optimize their scalability. Our approach tackles the issue of increasing degeneracy of the low energy states as systems scale up at the expense of longer total simulation time.

The reliability and efficiency of our method can be improved by employing a quantum oracle to prepare an initial state for the amplification stages with an overlap with the ground state larger than a certain threshold. Methods such as single ancilla-Lindbladian evolution [10] and Adiabatic Evolution [11, 12] can be tested as a pre-processing stage for the approach presented in this work. Another exciting direction could be employing classical algorithms such as DMRG [13, 14] or Coupled Cluster [15] to obtain an initial state. This state can then be prepared by the quantum hardware through known methods such as Ref. [16] proposed by Mottonen et al., by unitary dilation of the matrix product state tensors [17, 18], or sparsification methods [7].

Methods of efficiently implementing time evolution blocks with large time coefficients should be investigated [19] because the RPE algorithm we apply at the end of the amplification layers promises a high potential of enhancing the noise tolerance if we can prevent the depth of time evolution circuit from scaling linearly with increasing time coefficient.

On top of depolarizing noise, the effects of other noise models, such as amplitude damping [20, 21], dephasing error [22–24], coherent errors in the form of over-rotation [25, 26] and measurement noise [27–29] can be further investigated.

Possibly enhancing our method by combining it with other error correction methods, such as the noise estimation [30], randomized compiling [31] and using a coherent recovery sequence [25, 26] are interesting directions for future work.

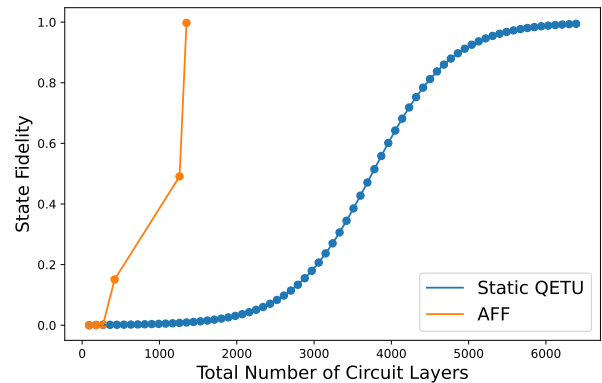


FIG. 6. Ground state preparation for TFIM with system size  $L = 10$ , for small initial overlap  $|\langle \psi | \psi_0 \rangle| \approx 10^{-7}$ . For the static application of QETU, we assume we have access to a perfect cut-off value  $\mu \in (a_1, a_0)$  (this strict assumption can be alleviated for AFF). "Total Number of Circuit Layers" represents the number of layers in the brick wall layout, used in RQC-Opt optimization to encode the time evolution operator, scaled by the polynomial degree  $\eta = 30$ . RQC-Opt needs only up to 7 layers per time evolution block if time coefficient  $t < 1$ . For the case  $t > 1$ , we split  $dt = \frac{t}{n}$ , such that  $dt < 1$  and repeat the circuit  $n$  times. It is remarkable that in the fifth filtering stage of the AFF approach, we use the largest number of circuit layers, but to reach  $|\langle \psi_0 | \psi_f \rangle| \approx 1$ , we need to apply the first filtering (with lowest  $t$  coefficient) again. This dampens the higher excited states once more and demonstrates the relative amplification between the ground and first excited states by the sixth stage of AFF.

## AUTHOR CONTRIBUTIONS

The authors confirm their contribution to the paper as follows: Study conception and design: E. Karacan, C. B. Mendl; Implementation and Simulation: E. Karacan; Analysis and interpretation of results: E. Karacan, C. B. Mendl; Draft Manuscript Preparation: E. Karacan, Y. Chen, C. B. Mendl. All authors reviewed the results and approved the final version of the manuscript.

## ACKNOWLEDGMENTS

We would like to thank L. Lin, Y. Dong and Z. Ding for insightful discussions during the conceptual development and implementation of this project. Y. Chen acknowledges funding by the Munich Quantum Valley section K7 (QACI), which is supported by the Bavarian state government with funds from the Hightech Agenda Bayern Plus.



### Appendix A: Circuit Depth Scaling for Static Repetition of QETU

In this section, we derive the result presented in Proposition II B. We will assume the non degenerate case for the ground and first excited states, which fits most of the use cases. For the degenerate case one can show the same end result. Firstly, we can write the relative amplification, defined in 1 as the following:

$$A = \frac{F(a_0)}{F(a_0 - \Delta_a)} \quad (\text{A1})$$

where  $\Delta_a := a_0 - a_1$  is the spectral gap in the cosine space. We then make the following approximation for the relative amplification (when static repetition approach is employed):

$$A_{\text{ST}} \approx \left( \frac{1 - (a_0 + 1)^{-\eta}}{1 - (a_0 + 1 - \Delta_a)^{-\eta}} \right)^\gamma \quad (\text{A2})$$

where  $\gamma$  is the number of consecutive, static repetitions of the QETU circuit. Here, the polynomial  $F(a)$  of degree  $\eta$  is approximated through:

$$F(a) \approx 1 - (a + 1)^{-\eta}. \quad (\text{A3})$$

This approximation assumes the pessimistic scenario that  $a_1 > \mu$ , indicating that  $F(a)$  is concave in the region around  $[a_1, a_0]$ . For the convex case, one can take  $F(a) \approx \nu \left(\frac{a}{\mu}\right)^\eta$  where  $\nu \in (0, 1)$ . This does not change the end result, so we will continue with the concave assumption. To further simplify  $A_{\text{ST}}$ , we use Maclaurin series expansion:

$$A_{\text{ST}} \approx \left( \frac{1 - (1 - \eta a_0 + \frac{\eta(\eta+1)}{2} a_0^2 + \dots)}{1 - (1 - \eta(a_0 - \Delta_a) + \frac{\eta(\eta+1)}{2} (a_0 - \Delta_a)^2 + \dots)} \right)^\gamma. \quad (\text{A4})$$

Resulting from  $a_0, a_0 - \Delta_a < 1$ , we further simplify the expression by ignoring the higher order terms as:

$$A_{\text{ST}} \approx \left( \frac{a_0}{a_0 - \Delta_a} \right)^\gamma \quad (\text{A5})$$

This approximation results in the following expression for  $\gamma = \gamma_{\text{ST}}$  and  $A_{\text{ST}} = \Theta\left(\frac{a_0}{\Delta_a \tilde{\epsilon}}\right)$  (as given in 7):

$$\gamma_{\text{ST}} \approx \frac{\log(1/A_{\text{ST}})}{\log(1 - \frac{\Delta_a}{a_0})} = \Theta\left(\frac{\log(\frac{\Delta_a \tilde{\epsilon}}{a_0})}{\log(1 - \frac{\Delta_a}{a_0})}\right) \quad (\text{A6})$$

We use the Taylor expansion of  $\log(1 + x) = x - \frac{x^2}{2} + \dots$  and obtain the following result:

$$\gamma_{\text{ST}} = \Theta\left(\frac{\log(\frac{\Delta_a \tilde{\epsilon}}{a_0})}{-\frac{\Delta_a}{a_0} - 0.5 \left(\frac{\Delta_a}{a_0}\right)^2 + \dots}\right) = \Theta\left(\frac{a_0}{\Delta_a} \cdot \log\left(\frac{a_0}{\Delta_a \tilde{\epsilon}}\right)\right) \quad (\text{A7})$$

We further aim to avoid the dependence of the above expression on  $\Delta_a$  by replacing it with an expression dependent on spectral gap in the eigenvalue space  $\Delta$ . For this purpose, we derive a relation between  $\Delta_a$  and  $\Delta$ :

$$\Delta_a = \cos\left(\frac{\lambda_0}{2}\right) - \cos\left(\frac{\lambda_1}{2}\right) \quad (\text{A8})$$

$$= -2 \sin\left(\frac{\lambda_0 + \lambda_1}{2}\right) \sin\left(\frac{\lambda_0 - \lambda_1}{2}\right) \quad (\text{A9})$$

$$= 2 \sin\left(\frac{\lambda_0 + \lambda_1}{2}\right) \sin\left(\frac{\Delta}{2}\right) \quad (\text{A10})$$

$$\approx \frac{\Delta(\lambda_1 + \lambda_0)}{2} = \Theta(\Delta) \quad (\text{A11})$$

where we use the special case for our (linear transformed) Hamiltonian  $\tilde{H}$ , that the spectrum is compressed into the  $(0, \pi)$  range. To ensure this property, we apply the linear transformation given in 2 as  $\tilde{H} = \frac{\pi}{\Lambda}(H - \lambda_{\text{LB}}I)$ , which (in practice) results in  $|\lambda_0|, |\lambda_1| \ll 1$ , justifying the approximation above.

By combining this relation and our result from A7, we finally achieve the following scaling:

$$\gamma_{\text{ST}} = \Theta(\Delta^{-1} \log(\Delta^{-1} \tilde{\epsilon}^{-1})). \quad (\text{A12})$$

### Appendix B: Circuit Depth Scaling for Adaptive Finer Filtering

In this section, we show that Algorithm 1 achieves circuit depth scaling  $\gamma_{\text{AFF}}$  as given in Eq. (16).

Similar to the approximation given in Eq. (A2), we approximate the amplification that can be achieved by Adaptive Finer Filtering as:

$$A_{\text{AFF}} \approx \left( \frac{1 - (a_0 + 1)^{-\eta}}{1 - (a_0 + 1 - \tilde{\gamma}\Delta_a)^{-\eta}} \right) \quad (\text{B1})$$

where the same approximation for  $F(a)$  as in Eq. (A3) is used and  $\tilde{\gamma} < \frac{a_0}{\Delta_a}$  is the "stretch parameter" in the cosine space, that is related to the spectral gap as:

$$\begin{aligned} \tilde{\gamma}\Delta_a &= \cos\left(\frac{\gamma\lambda_0}{2}\right) - \cos\left(\frac{\gamma\lambda_1}{2}\right) \\ &= -2\sin\left(\frac{(\lambda_0 + \lambda_1)\gamma}{2}\right)\sin\left(\frac{(\lambda_0 - \lambda_1)\gamma}{2}\right). \end{aligned} \quad (\text{B2})$$

Here  $\gamma$  is the stretch parameter in the eigenvalue space, hence  $\gamma$  is also what we take as the circuit depth (in accordance to Def. 3).

We first consider the range of  $\tilde{\gamma}$ , in order to achieve the targeted relative amplification. By Eq. (B1) and using the same steps as in (A4) and (A5), we obtain:

$$A_{\text{AFF}} \approx \left( \frac{1 - (1 - \eta a_0 + \frac{\eta(\eta+1)}{2} a_0^2 + \dots)}{1 - (1 - \eta(a_0 - \tilde{\gamma}\Delta_a) + \frac{\eta(\eta+1)}{2} (a_0 - \tilde{\gamma}\Delta_a)^2 + \dots)} \right) \approx \frac{a_0}{a_0 - \tilde{\gamma}\Delta_a} \quad (\text{B3})$$

This approximation results in the following expression for  $\tilde{\gamma} = \tilde{\gamma}_{\text{AFF}}$  and  $A_{\text{AFF}} = \Theta\left(\frac{a_0}{\Delta_a \tilde{\epsilon}}\right)$  (as given in 7):

$$1 - \frac{\Delta_a \tilde{\gamma}_{\text{AFF}}}{a_0} = \Theta\left(\frac{\Delta_a \tilde{\epsilon}}{a_0}\right) \quad (\text{B4})$$

$$\tilde{\gamma}_{\text{AFF}} = \Theta\left(\frac{a_0}{\Delta_a} - \tilde{\epsilon}\right) \quad (\text{B5})$$

In order to derive the scaling for the circuit depth  $\gamma$ , we numerically simulate the relation between  $\tilde{\gamma}$  and  $\gamma$  for  $\tilde{\gamma} \approx \frac{a_0}{\Delta_a}$ . This is necessary because, unlike the assumptions made in Eq. (A8), we cannot take the arguments of sine terms in Eq (B2) to be small enough to justify a linear approximation of the sine function. As the result of the numerical simulation, we observe a linear scaling as:

$$\tilde{\gamma}\Delta_a = \Theta(\gamma\Delta) \quad (\text{B6})$$

The example plots for the numerical simulation are presented in Fig. 7. By using the result from B5, B6 and  $\Delta_a^{-1} \gg \tilde{\epsilon}$ , we finally obtain the scaling as:

$$\gamma_{\text{AFF}} = \Theta(\Delta^{-1}). \quad (\text{B7})$$

### Appendix C: Direct Expectation Value Measurement

The most straightforward idea of extracting the ground state energy information from the prepared ground state is to directly conduct measurements on the ground state to approximate the probability distribution of the state vector. This works in cases where the expectation value of the energy can be decomposed into a combination of Pauli operations, which corresponds to calculating the expectation value of the ground state w.r.t. a different measurement basis. This approach inevitably faces a stochastic limit as approximating the probability distribution with high precision for large systems is impossible with a sensible amount of experiments. Hence, the lower bound of approximation error significantly increases with growing system size, even in the ideal, noiseless case.

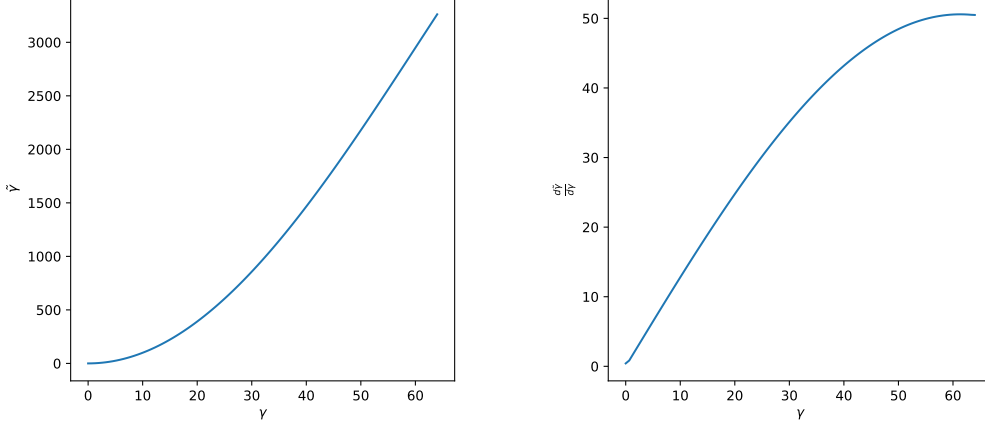


FIG. 7. Numerical simulation plots demonstrating the relation between  $\tilde{\gamma}$  and  $\gamma$  according to B2. Eigenvalues ( $\lambda_0, \lambda_1$ ) are set to (0.01, 0.05) to match the spectrum of the linearly scaled Hamiltonian (as given in Eq. (2)). We observe a quadratic scaling for small  $\tilde{\gamma}$  values, however scaling becomes linear in the range we operate ( $\tilde{A} = \frac{a_0}{\Delta_a \tilde{\epsilon}}$  indicating  $\tilde{\gamma} \approx \frac{a_0}{\Delta_a} > 3000$ ).

For the TFIM Hamiltonian, this corresponds to:

$$\begin{aligned}
 E_0 &= \langle \psi_0 | H_{\text{TFIM}} | \psi_0 \rangle = -J \sum_{j=1}^{L-1} \langle \psi_0 | Z_j Z_{j+1} | \psi_0 \rangle - g \sum_{j=1}^L \langle \psi_0 | X_j | \psi_0 \rangle \\
 &= -J \sum_{j=1}^{L-1} \sum_{\sigma_j=0}^1 \sum_{\sigma_{j+1}=0}^1 (-1)^{\sigma_j} (-1)^{\sigma_{j+1}} \mathbb{P}_Z(\sigma_j, \sigma_{j+1} | \psi_0) - g \sum_{j=1}^L \sum_{\sigma_j=0}^1 (-1)^{\sigma_j} \mathbb{P}_X(\sigma_j | \psi_0)
 \end{aligned} \tag{C1}$$

where  $\mathbb{P}_X(\sigma_j | \psi_0)$  is the probability of measuring  $j^{\text{th}}$  qubit as  $|\sigma_j\rangle$  on the  $X$ -basis and  $\mathbb{P}_Z(\sigma_j, \sigma_{j+1} | \psi_0)$  is the probability of measuring  $j^{\text{th}}$  and  $(j+1)^{\text{th}}$  qubits as  $|\sigma_j \sigma_{j+1}\rangle$  on the computational basis ( $Z$ -basis).

The simulation of conducting measurements w.r.t. a different basis than the computational basis is performed by applying a Hadamard gate to all the qubits for the  $X$ -measurement, as a consequence of  $X = HZH$ .

#### Appendix D: Robust Phase Estimation (RPE)

The Robust Phase Estimation algorithm, as proposed by Ni et al. [4], approximates the ground state energy from an end state whose overlap with the ground state is large enough ( $> 0.53$ ) digit by digit on the binary basis, by employing the same Hadamard circuit, as the one given in Fig. 4, whose time coefficient is set to  $t = 2^j$ , where  $j$  is the target digit the search aims to identify. By successively increasing  $j$  and using the result from the predecesing search stage, RPE enables highly noise-resilient and robust approximation of the ground state energy, especially if the initial overlap is high  $\approx 1$ .

We start with a rough estimate  $\theta_{-1}$ , that can be acquired through methods such as DEM (Appendix C) and follow the given Algorithm 3: This method is remarkable due to its short circuit depth, overcoming the stochastic sampling

---

#### Algorithm 3: Robust Phase Estimation (RPE)

(proposed by Ni et al. [4])

---

**Data:**  $|\psi\rangle, \theta_{-1}, J, N_S$

**for**  $j = 0, \dots, J-1$  **do**

$Z_j \approx \langle \psi | e^{i2^j H} | \psi \rangle$  // Acquired through the Hadamard test circuit in Fig. 4 with  $N_S$  samples

$S_j := \left\{ \frac{2k\pi + \arg Z_j}{2^j} \right\}_{k=0, \dots, 2^j-1}$

$\theta_j = \arg \min_{\theta \in S_j} [\pi - |(\theta - \theta_{j-1}, \text{mod } 2\pi) - \pi|]$

**end**

**return**  $\theta_{J-1}$

---

limitations (Monte-Carlo noise), and high performance despite small sampling size  $N_S \in [10^2, 10^3]$ . This method also tolerates local depolarizing noise well. For further details, please refer to [4].

### Appendix E: Quantum Complex Exponential Least Squares (QCELS) Algorithm

Another ground state energy estimation algorithm we use in our benchmarks is the Quantum Complex Exponential Least Squares Algorithm (QCELS), as proposed by Ding et al. [5].

In this Algorithm, the same Hadamard test circuit (Fig. 4), with the number of samples  $N_S$ , is employed to estimate a set of phases  $\{Z_n\}_{n=0}^{N-1}$ :

$$Z_n \approx e^{-i\lambda_0 t_n} \quad (\text{E1})$$

for different  $t_n$  values:  $t_n = n\tau_j$ , where  $\tau_j$  gets successively higher as  $\tau_j = \tau \cdot 2^j$ , for  $j = 0, \dots, J-1$ . Here  $J, N_S, \tau$  and  $N$  are constants to be set depending on system parameters.

On this data set  $\{Z_n\}_{n=0}^{N-1}$ , we perform an exponential fit ( $r e^{-i\theta t_n}$ ) at each stage  $j$  and choose the optimal angle parameter  $\theta_j^*$  as the result of the current stage. Next stage  $j+1$  continues the optimization within the bounds limited by  $(\theta_j^* - \frac{\pi}{2\tau_j}, \theta_j^* + \frac{\pi}{2\tau_j})$  with an increased time step  $\tau_{j+1} = 2\tau_j$ . For the results displayed in Table II, we used  $N = 5$ ,  $\tau = 0.2$ ,  $J = 9$ ,  $N_S = 10^4$ , so that the maximal simulation time  $T_{\max}$  matches the  $T_{\max}$  of RPE (Appendix D). This algorithm is summarized in Alg. 4.

---

#### Algorithm 4: Quantum Complex Exponential Least Squares (QCELS) Algorithm (proposed by Ding et al. [5])

---

```

Data:  $|\psi\rangle, \lambda_{LB}, \lambda_{UB}, J, N_S, N, \tau$ 
for  $j = 0, \dots, J-1$  do
     $\tau_j \leftarrow \tau \cdot 2^j$ 
     $\{Z_{j,n}\}_{n=0}^{N-1} \approx \{\langle \psi | e^{in\tau_j H} | \psi \rangle\}_{n=0}^{N-1}$  // Acquired through the circuit in Fig. 4 with  $N_S$  samples
     $\theta_j^* \leftarrow \arg \min_{r \in \mathbb{C}, \theta \in [\lambda_{LB}, \lambda_{UB}]} \frac{1}{N} \sum_{n=0}^{N-1} |Z_{j,n} - r e^{-i\theta n\tau_j}|^2$ 
     $(\lambda_{LB}, \lambda_{UB}) \leftarrow (\theta_j^* - \frac{\pi}{2\tau_j}, \theta_j^* + \frac{\pi}{2\tau_j})$ 
end
return  $\theta_{J-1}$ 

```

---

### REFERENCES

- [1] Y. Dong, L. Lin, and Y. Tong, Ground-state preparation and energy estimation on early fault-tolerant quantum computers via quantum eigenvalue transformation of unitary matrices, PRX Quantum **3**, 040305 (2022).
- [2] J. M. Martyn, Z. M. Rossi, A. K. Tan, and I. L. Chuang, Grand unification of quantum algorithms, PRX Quantum **2**, 040203 (2021).
- [3] A. Kotil, R. Banerjee, Q. Huang, and C. B. Mendl, Riemannian quantum circuit optimization for Hamiltonian simulation, J. Phys. A: Math. Theor. **57**, 135303 (2024).
- [4] H. Ni, H. Li, and L. Ying, On low-depth algorithms for quantum phase estimation, Quantum **7**, 1165 (2023).
- [5] Z. Ding and L. Lin, Even shorter quantum circuit for phase estimation on early fault-tolerant quantum computers with applications to ground-state energy estimation, PRX Quantum **4**, 020331 (2023).
- [6] L. Lin and Y. Tong, Heisenberg-limited ground-state energy estimation for early fault-tolerant quantum computers, PRX Quantum **3**, 10.1103/prxquantum.3.010318 (2022).
- [7] O. Kiss, U. Azad, B. Requena, A. Roggero, D. Wakeham, and J. M. Arrazola, Early fault-tolerant quantum algorithms in practice: Application to ground-state energy estimation (2024), arXiv:2405.03754 [quant-ph].
- [8] L. Lin and Y. Tong, Near-optimal ground state preparation, Quantum **4**, 372 (2020).
- [9] E. Karacan, Adaptive finer filtering for ground state preparation.
- [10] Z. Ding, C.-F. Chen, and L. Lin, Single-ancilla ground state preparation via Lindbladians, arXiv:2308.15676 (2023), arXiv:2308.15676 [quant-ph].
- [11] T. Albash and D. A. Lidar, Adiabatic quantum computation, Reviews of Modern Physics **90**, 10.1103/revmodphys.90.015002 (2018).
- [12] C. M. Keever and M. Lubasch, Towards adiabatic quantum computing using compressed quantum circuits (2023), arXiv:2311.05544 [quant-ph].
- [13] S. R. White, Density matrix formulation for quantum renormalization groups, Phys. Rev. Lett. **69**, 2863 (1992).
- [14] K. G. Wilson, The renormalization group: Critical phenomena and the kondo problem, Rev. Mod. Phys. **47**, 773 (1975).
- [15] R. J. Bartlett and M. Musiał, Coupled-cluster theory in quantum chemistry, Rev. Mod. Phys. **79**, 291 (2007).

- [16] M. Mottonen, J. J. Vartiainen, V. Bergholm, and M. M. Salomaa, Transformation of quantum states using uniformly controlled rotations (2004), arXiv:quant-ph/0407010 [quant-ph].
- [17] A. Smith, B. Jobst, A. G. Green, and F. Pollmann, Crossing a topological phase transition with a quantum computer, *Phys. Rev. Res.* **4**, L022020 (2022).
- [18] D. Malz, G. Styliaris, Z.-Y. Wei, and J. I. Cirac, Preparation of matrix product states with log-depth quantum circuits, *Phys. Rev. Lett.* **132**, 040404 (2024).
- [19] C. Mc Keever and M. Lubasch, Classically optimized Hamiltonian simulation, *Phys. Rev. Res.* **5**, 023146 (2023).
- [20] M. A. Nielsen and I. L. Chuang, *Quantum Computation and Quantum Information* (Cambridge University Press, 2010).
- [21] M. A. Aziz, B. P. Gond, S. Nandi, S. Ray, D. Bhoomik, and R. Majumdar, Thermal relaxation error on QKD: effect and a probable bypass, arXiv:2207.01159 (2022), arXiv:2207.01159 [quant-ph].
- [22] I. L. Chuang, R. Laflamme, P. W. Shor, and W. H. Zurek, Quantum computers, factoring, and decoherence, *Science* **270**, 1633 (1995).
- [23] A. Barenco, A. Ekert, K.-A. Suominen, and P. Törmä, Approximate quantum Fourier transform and decoherence, *Phys. Rev. A* **54**, 139 (1996).
- [24] W. G. Unruh, Maintaining coherence in quantum computers, *Phys. Rev. A* **51**, 992 (1995).
- [25] A. K. Tan, Y. Liu, M. C. Tran, and I. L. Chuang, Error correction of quantum algorithms: arbitrarily accurate recovery of noisy quantum signal processing, arXiv:2301.08542 (2023), arXiv:2301.08542 [quant-ph].
- [26] A. K. Tan, Y. Liu, M. C. Tran, and I. L. Chuang, Perturbative model of noisy quantum signal processing, *Phys. Rev. A* **107**, 042429 (2023).
- [27] F. Wudarski, Y. Zhang, and M. I. Dykman, Nonergodic measurements of qubit frequency noise, *Phys. Rev. Lett.* **131**, 230201 (2023).
- [28] F. Wudarski, Y. Zhang, A. N. Korotkov, A. G. Petukhov, and M. I. Dykman, Characterizing low-frequency qubit noise, *Phys. Rev. Applied* **19**, 064066 (2023).
- [29] B. Nachman, M. Urbanek, W. A. de Jong, and C. W. Bauer, Unfolding quantum computer readout noise, *npj Quantum Inf.* **6**, 84 (2020).
- [30] M. Urbanek, B. Nachman, V. R. Pascuzzi, A. He, C. W. Bauer, and W. A. de Jong, Mitigating depolarizing noise on quantum computers with noise-estimation circuits, *Phys. Rev. Lett.* **127**, 270502 (2021).
- [31] A. Hashim, R. K. Naik, A. Morvan, J.-L. Ville, B. Mitchell, J. M. Kreikebaum, M. Davis, E. Smith, C. Iancu, K. P. O'Brien, I. Hincks, J. J. Wallman, J. Emerson, and I. Siddiqi, Randomized compiling for scalable quantum computing on a noisy superconducting quantum processor, *Phys. Rev. X* **11**, 041039 (2021).